# Formation and detection of a chiral orbital Bose liquid in an optical lattice

Xiaopeng Li,[1, 2] Arun Paramekanti,[3, 4] Andreas Hemmerich,[5] and W. Vincent Liu[1, 6]

[1]*Department of Physics and Astronomy, University of Pittsburgh, Pittsburgh, Pennsylvania 15260, USA*
[2]*Kavli Institute for Theoretical Physics, University of California, Santa Barbara, CA 93106, USA*
[3]*Department of Physics, University of Toronto, Toronto, Ontario M5S 1A7, Canada*
[4]*Canadian Institute for Advanced Research, Toronto, Ontario M5G 1Z8, Canada*
[5]*Institut für Laser-Physik, Universität Hamburg, Luruper Caussee 149, 22761 Hamburg, Germany*
[6]*Center for Cold Atom Physics, Chinese Academy of Sciences, Wuhan 430071, China*

**Recent experiments [1, 2] on $p$-orbital atomic bosons have suggested the emergence of a spectacular ultracold superfluid with staggered orbital currents in optical lattices. This raises fundamental questions like the effects of collective thermal fluctuations, and how to directly observe such chiral order. Here, we show via Monte Carlo simulations that thermal fluctuations destroy this superfluid in an unexpected two-step process, unveiling an intermediate normal phase with spontaneously broken time-reversal symmetry, dubbed "chiral Bose liquid". For integer fillings ($n \geq 2$) in the chiral Mott regime [3], thermal fluctuations are captured by an effective orbital Ising model, and Onsager's powerful exact solution [4] is adopted to determine the transition from this intermediate liquid to the para-orbital normal phase at high temperature. A suitable lattice quench is designed to convert the staggered angular momentum, previously thought by experts difficult to directly probe, into coherent orbital oscillations, providing a smoking-gun signature of chiral order.**

Orbital degrees of freedom and interactions play a crucial role in the emergence of many complex phases in solid state materials. High temperature superconductivity in the cuprates [5] and pnictides [6], colossal magnetoresistance observed in Mn oxides [7], and chiral p-wave superconductivity proposed in $Sr_2RuO_4$ [8], are all nucleated by strong correlation effects in a multi-orbital setting [9]. For ultracold atomic gases, interaction effects combined with the band topology of $p$-orbitals [10] has been argued to lead to exotic topological or superfluid (SF) phases for fermions [11–17] as well as bosons [1, 3, 18–27]. Interactions are predicted to drive a semi-metal to topological insulator quantum phase transition in two dimensions (2D) for fermions in $p_x$, $p_y$ and $d_{x^2-y^2}$ orbitals [16], while interacting $p$-orbital atomic fermions in 3D could lead to axial orbital order [28]. For weakly interacting 2D lattice bosons in $p_x$ and $p_y$-orbitals the ground state is proposed to be a SF with staggered $p_x \pm ip_y$ order [19]; such order is also found for 1D strongly interacting $p$-orbital bosons [26]. For bosons, these exotic phases can result from a particularly simple effect: repulsive contact interactions favor a maximization of the local angular momentum $\mathcal{L}_z$, a bosonic variant of the atomic Hund's rule for electrons [3, 19, 27].

While previous work has focused on the ground state properties of such unconventional Bose SFs, here we address two important outstanding issues. (i) How do thermal or quantum fluctuations, which are important in any experimental setting, melt these unconventional SF states? (ii) How can one directly detect the spatially modulated angular momentum underlying these unusual quantum states?

Our work is motivated by recent experiments which have successfully prepared long-lived metastable phases of weakly interacting $^{87}$Rb atoms in $p$-orbitals [1, 2]. In the deep lattice regime, this experimental system is well approximated by a tight binding model on a checkerboard optical lattice with bosons in the $p_x$, $p_y$ and $s$ orbital degrees of freedom (see Fig. 1). The Hamiltonian of the model is obtained by extending the early theoretical studies [3, 18, 19, 29] to the checkerboard lattice configuration used in the recent experiments of Ref. [1, 2]. Restricting ourselves to nearest-neighbor tunneling, we find $H = H_{\text{tun}} + H_{\text{loc}}$, with tunneling and local terms,

$$H_{\text{tun}} = -\frac{t}{\sqrt{2}} \sum_{\mathbf{r}} \left\{ \left[ b_x^\dagger(\mathbf{r}) + b_y^\dagger(\mathbf{r}) \right] \left[ b_s(\mathbf{r}_1) - b_s(\mathbf{r}_2) \right] \right.$$
$$\left. + \left[ b_y^\dagger(\mathbf{r}) - b_x^\dagger(\mathbf{r}) \right] \left[ b_s(\mathbf{r}_3) - b_s(\mathbf{r}_4) \right] + h.c. \right\} \quad (1)$$

$$H_{\text{loc}} = -\sum_{\mathbf{r}} \left[ \mu_p n_p(\mathbf{r}) + \mu_s n_s(\mathbf{r}_1) \right]$$
$$+ \sum_{\mathbf{r}} \frac{U_p}{2} \left\{ n_p(\mathbf{r}) \left[ n_p(\mathbf{r}) - \frac{2}{3} \right] - \frac{1}{3} \mathcal{L}_z^2(\mathbf{r}) \right\}$$
$$+ \sum_{\mathbf{r}} \frac{U_s}{2} n_s(\mathbf{r}_1) \left[ n_s(\mathbf{r}_1) - 1 \right]. \quad (2)$$

Here, $b_x(\mathbf{x})$, $b_y(\mathbf{x})$ and $b_s(\mathbf{x})$ are bosonic annihilation operators of $p_x$, $p_y$ and $s$ orbitals at site $\mathbf{x}$. The position vectors $\mathbf{r} = r_x \hat{a}_x + r_y \hat{a}_y$, with integers $r_x$ and $r_y$. The vector $\hat{a}_x$ ($\hat{a}_y$) is the primitive vector of the square lattice in the $x$ ($y$) direction (Fig. 1). The positions of $s$ orbitals are $\mathbf{r}_1 = \mathbf{r} + \frac{\hat{a}_x + \hat{a}_y}{2}$, $\mathbf{r}_2 = \mathbf{r} - \frac{\hat{a}_x + \hat{a}_y}{2}$, $\mathbf{r}_3 = \mathbf{r} - \frac{\hat{a}_x - \hat{a}_y}{2}$, and $\mathbf{r}_4 = \mathbf{r} + \frac{\hat{a}_x - \hat{a}_y}{2}$. The density operators are defined as $n_p = b_x^\dagger b_x + b_y^\dagger b_y$ and $n_s = b_s^\dagger b_s$. The angular momentum operator is

$$\mathcal{L}_z = i(b_x^\dagger b_y - b_y^\dagger b_x). \quad (3)$$

Here, we have assumed square lattice $C_4$ rotational symmetry.

With an analysis of the time-of-flight momentum distribution, the researchers in [1, 2] found evidence suggesting a staggered $p_x \pm i p_y$ SF. However, a direct measurement of its key property — the angular momentum order — remains a challenge. This is especially crucial in the absence of superfluid coherence, since quantum or thermal fluctuations may kill superfluidity while preserving angular momentum order. Such fluids with spontaneously broken time-reversal symmetry but no superfluidity, are also thought to be relevant to $Sr_2RuO_4$ [30–32], and to the pseudogap state of the high temperature superconductors [33–35].

## Results

This brings us to two central results. (i) Using classical Monte Carlo simulations of an effective model of interacting $p_x$ and $p_y$ bosons, we show that thermal fluctuations lead to a two-step melting of the staggered $p_x \pm i p_y$ superfluid ground state. Sandwiched between a lower temperature Berezinskii-Kosterlitz-Thouless (BKT) transition at which superfluidity is lost, and a higher temperature Ising transition at which time-reversal symmetry is restored, lies a "chiral Bose liquid" with spontaneously broken time-reversal symmetry. In other words, *it is a remarkable state of matter that is chiral but not superfluid.* For large Hubbard repulsion at integer fillings, $n \geq 2$, a strong coupling expansion yields Mott insulating states with staggered $p_x \pm i p_y$-order. As shown schematically in Fig. 1, this opens up a wide window in the phase diagram where staggered angular momentum order persists robustly even in the absence of superfluidity.

(ii) Mapping the $p_x, p_y$ orbitals onto an effective pseudospin-1/2 degree of freedom, we show that one can simulate the spin dynamics in magnetic solids by orbital dynamics of $p$-band bosons. Specifically, we numerically study a particular lattice quench, using time-dependent matrix product and Gutzwiller states, which is shown to convert the angular momentum order of such chiral fluids into time-dependent oscillations of the orbital population imbalance, analogous to Larmor spin precession. These oscillations directly reveal the experimentally hard-to-detect "hidden order" associated with spontaneous time-reversal symmetry breaking. This quench is analogous to nuclear magnetic resonance schemes in liquids or solids, which tip the nuclear moment vector and study its subsequent precession using radio-frequency probes. This non-interferometric route to measuring the angular momentum order works in superfluid as well as non-superfluid regimes, and it could be implemented using recent experimental innovations [36–38].

**Strong Coupling:** $p_x \pm i p_y$ **Mott Insulator and Chiral Bose Liquid.** We begin with the strong coupling regime, where atoms can localize to form a Mott insulator (MI) ground state. When the $s$-orbitals in one of
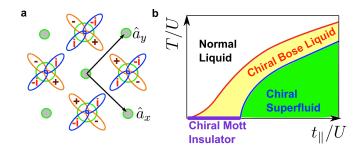


FIG. 1: Orbital lattice structure and phase diagram. (**a**), the checkerboard lattice structure as used in experiments to realize $p$-orbital superfluid [1], together with the phases of the staggered orbital ordering in chiral states. (**b**) shows the phase diagram of $p$-orbital band Bosons with filling $n \geq 2$. The diagram is fixed by exact or controlled numerical and analytical calculations in the strong and weak coupling limits at non-zero temperature and for arbitrary coupling along the $T = 0$ line of "Chiral Mott" and is otherwise interpolated schematically elsewhere. At zero temperature there is a quantum phase transition between the chiral Mott insulator and superfluid phases, both of which break time reversal symmetry. At finite temperature, there is a chiral Bose liquid phase. Upon heating, the chiral superfluid undergoes a BKT transition into the chiral Bose liquid, which subsequently undergoes an Ising transition at a higher temperature into a normal Bose liquid.

the sublattices (Fig. 1) are largely mismatched in energy with the $p$-orbitals, with a gap $\Delta_{sp}$, the nearest-neighbor tunneling Hamiltonian for bosons dominantly residing in the $p$-orbitals is given by

$$
\begin{aligned}
H_{tun}^{eff} = & \sum_{\mathbf{r}} \left\{ t_\parallel \left[ b_x^\dagger(\mathbf{r}) b_x(\mathbf{r} + \hat{a}_x) + x \leftrightarrow y \right] \right. \\
& \left. - t_\perp \left[ b_x^\dagger(\mathbf{r}) b_x(\mathbf{r} + \hat{a}_y) + x \leftrightarrow y \right] + h.c. \right\}, \quad (4)
\end{aligned}
$$

with hopping amplitudes $t_\parallel \approx t_\perp \approx \frac{t^2}{\Delta_{sp}}$ being mediated by the $s$-orbitals. At integer filling, with $n \geq 2$, a strong $p$-orbital Hubbard repulsion in Eq. (2) favors a local state with a fixed particle number with nonzero angular momentum in order to minimize the interaction energy [3, 26, 27, 29], leading to a Mott insulator with a two-fold degeneracy of orbital states $p_x \pm i p_y$ at each site. This extensive degeneracy is lifted by virtual boson fluctuations within second order perturbation theory in the boson hopping amplitudes. This effect is captured, by setting $\mathcal{L}_z(\mathbf{r}) = \sigma_z(\mathbf{r}) |\mathcal{L}_z(\mathbf{r})|$, and deriving an effective exchange Hamiltonian between the Ising degrees of freedom $\sigma_z(\mathbf{r})$,

$$
H_{Ising}^{eff} = \sum_{\langle \mathbf{r}, \mathbf{r}' \rangle} \mathcal{J} \sigma_z(\mathbf{r}) \sigma_z(\mathbf{r}'), \quad (5)
$$

where $\mathcal{J} = \frac{3n^2(n+2)}{2(n+1)} \frac{t_\parallel t_\perp}{U} > 0$. The chiral MI ground state thus supports a staggered (antiferromagnetic) angular momentum pattern, with a nonzero order parameter $\mathcal{L}_z^{stag}(\mathbf{r}) = (-1)^{r_x + r_y} \mathcal{L}_z(\mathbf{r})$ out to arbitrarily strong

coupling. Such staggered time-reversal symmetry broken Mott insulators, albeit for far more delicate *plaquette* currents, are known to emerge in frustrated Bose Hubbard models without orbital degrees of freedom, but only in an extremely small parameter window of interactions [39–41]. As schematically shown in Fig. 1, heating this MI leads to a "chiral Bose liquid" with spontaneously broken time-reversal symmetry. It only reverts to a conventional normal fluid above a symmetry restoring thermal phase transition of $H_{\text{Ising}}^{\text{eff}}$ which occurs at $k_B T_I \approx 2.27\mathcal{J}$ [4].

**Weak Coupling: Monte Carlo Simulations.** At weak coupling, we begin with the Hamiltonian $H_{\text{tun}}^{\text{eff}}$, supplemented with local $p$-orbital interactions

$$
\begin{aligned}
H_{\text{loc}}^{\text{eff}} = & \sum_{\mathbf{r}} \frac{U_p}{2} \left\{ n_p(\mathbf{r}) \left[ n_p(\mathbf{r}) - \frac{2}{3} \right] - \frac{1}{3} \mathcal{L}_z^2(\mathbf{r}) \right\} \\
& - \sum_{\mathbf{r}} \mu_p n_p(\mathbf{r}).
\end{aligned} \tag{6}
$$

For small $U_p \ll t_\parallel, t_\perp$, the band structure of $p$-band bosons has minima at $(\pi, 0)$ and $(0, \pi)$. Interactions scatter boson pairs from one minimum into the other, leading the bosons to condense into a superposition state of the two modes, phase-locked with a relative phase $\pm\pi/2$. This gives rise to a $p_x \pm ip_y$ superfluid ground state with a spontaneously broken time-reversal symmetry and nonzero staggered angular momentum order.
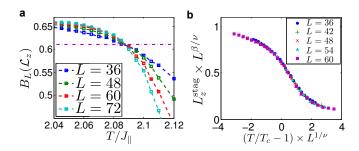
FIG. 2: Monte Carlo simulation results for the angular momentum ordering of the $p_x \pm ip_y$ superfluid. (**a**), Binder cumulant $B_L(\mathcal{L}_z)$ of the staggered angular momentum order parameter for different system sizes $L$ showing a crossing point at the Ising transition at $T/J_\parallel = 2.088(3)$. The dashed line indicates the critical Binder cumulant $0.61069\ldots$ for a 2D Ising transition. (**b**), scaling collapse of the angular momentum order parameter curves for Ising exponents $\nu = 1$ and $\beta = 1/8$.

To study the impact of thermal fluctuations on this weakly correlated superfluid, we make the reasonable assumption that classical phase fluctuations dominate the universal physics in the vicinity of the thermal phase transitions of this superfluid. This allows us to ignore the subdominant density fluctuations, and to replace $b_{x,y}^\dagger \sim \sqrt{\rho/2}e^{i\theta_{x,y}}$, with $\rho$ being the boson density, ar-
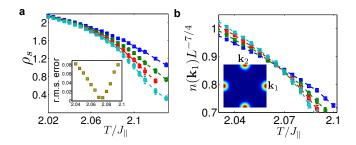
FIG. 3: Monte Carlo simulation results for the superfluidity of $p$-orbital bosons. (**a**), temperature dependence of the superfluid stiffness $\rho_s$ for different system sizes $L$, showing a rapid drop consistent with finite size effects at a BKT transition. Inset shows the r.m.s. error from fitting $\rho_s(L)$ to the Weber-Minnhagen log-scaling form at different temperatures, with a steep minimum at the BKT transition point $T/J_\parallel = 2.072(3)$. (**b**), scaled momentum distribution $n(\mathbf{k}_1)L^{-7/4}$ for different system sizes $L$, showing a crossing at the BKT transition point. Inset shows the schematic momentum distribution over the Brillouin zone, with equal height peaks at $\mathbf{k}_1$ and $\mathbf{k}_2$.

riving at an effective classical phase-only Hamiltonian

$$
\begin{aligned}
H_{\text{phase}}^{\text{eff}} = & \sum_{\mathbf{r}} \left[ \left\{ 2J_\parallel \cos(\Delta_x \theta_x(\mathbf{r})) - 2J_\perp \cos(\Delta_y \theta_x(\mathbf{r})) \right\} \right. \tag{7} \\
& + \left. \{x \leftrightarrow y\} \right] - U \sum_{\mathbf{r}} \sin^2(\theta_x(\mathbf{r}) - \theta_y(\mathbf{r})) \tag{8}
\end{aligned}
$$

where $\Delta_j \theta_\alpha(\mathbf{r}) = \theta_\alpha(\mathbf{r} + \hat{a}_j) - \theta_\alpha(\mathbf{r})$ with $j = x, y$, $J_{\parallel,\perp} \approx \rho t_{\parallel,\perp}/2$ and $U \approx \rho^2 U_p/6$.

Using Monte Carlo simulations (see Methods), we have studied the thermal phase diagram of this model for fixed values of $U/J_\parallel$, with $J_\perp/J_\parallel = 1$. As shown in Fig. 2, the Binder cumulant [42] $B_L(\mathcal{L}_z)$ for the staggered angular momentum order, computed for $U/J_\parallel = 1$ on $L \times L$ systems with various $L$, exhibits a unique crossing point at $T/J_\parallel = 2.088(3)$, signaling a critical point with a diverging correlation length. The critical value of this Binder cumulant is $B^* \approx 0.61$, very close to the universal 2D Ising value $\approx 0.61069$ for the aspect ratio of unity and periodic boundary conditions used in our simulations. This suggests that the staggered angular momentum order disappears at $T_I/J_\parallel = 2.088(3)$ via a thermal transition in the 2D Ising universality class. In order to track the destruction of superfluidity, we have computed the superfluid stiffness $\rho_s$ (see Methods), finding evidence of a Berezinskii-Kosterlitz-Thouless type behavior rounded by finite size effects. A finite size scaling analysis shows that a fit to the Weber-Minnhagen log-scaling form [43], obtained from the Kosterlitz-Thouless renormalization group equations, yields $T_{\text{BKT}}/J_\parallel = 2.072(3)$. An unbiased fit to this log-scaling form also yields $\rho_s(T_{\text{BKT}})/T_{\text{BKT}} \approx 0.64$, very close to the universal value $2/\pi$. As further confirmation of the BKT character of the superfluid transition, we have computed the boson momentum distribution

$n(\mathbf{k}) = \frac{1}{L^2}\sum_{\mathbf{r},\mathbf{r'},\alpha} e^{i\mathbf{k}\cdot(\mathbf{r}-\mathbf{r'})}\langle e^{i\theta_\alpha(\mathbf{r})}e^{-i\theta_\alpha(\mathbf{r'})}\rangle$, finding equal height peaks at $\mathbf{k}_1 = (\pi,0)$ and $\mathbf{k}_2 = (0,\pi)$. This is consistent with the weak coupling analysis which shows $p$-band dispersion minima at these momenta. At a BKT transition, the momentum distribution is expected to scale as $\sim L^{7/4}$ (in contrast to scaling as $\rho_c L^2$ for a Bose condensate with a condensate density $\rho_c$). This implies that the scaled momentum distributions $n(\mathbf{k}_1)L^{-7/4}$ cross at $T_{\mathrm{BKT}}$ for various system sizes $L$; we find this occurs at $T/J_\parallel \approx 2.07$, close to the result found from the superfluid stiffness analysis (Fig. 3). Our numerical study thus shows that the $p_x \pm ip_y$ superfluid undergoes a two-step destruction: a lower temperature BKT transition at which superfluidity is lost followed by a higher temperature Ising transition at which time reversal symmetry is restored, leading to an unconventional "chiral Bose liquid" at intermediate temperatures $2.072(3) \lesssim T \lesssim 2.088(3)$. With increasing correlations, the BKT transition temperature is expected to get suppressed, eventually vanishing at the Mott transition (for integer fillings $n \geq 2$), while the Ising transition remains nonzero for arbitrarily large repulsion as seen from the earlier strong coupling limit. Correlation effects thus enhance the window where one realizes a "chiral Bose liquid" as shown in the schematic temperature-interaction phase diagram in Fig. 1.

**Quantum Quench and Single-Site Orbital Dynamics.** One can draw a fruitful analogy between the two orbital states at each site $p_x, p_y$ and a pseudospin-1/2 degree of freedom $\uparrow, \downarrow$. This suggests that one can simulate spin dynamics in solid state materials by studying orbital dynamics of $p$-band bosons. As we will see, this also suggests a route to directly detecting the angular momentum order in the $p_x \pm ip_y$ superfluid and "chiral Bose liquid" of the type we have obtained. In our analogy, the $p_x \pm ip_y$ state corresponds to a pseudospin pointing along the $\pm\hat{y}$ direction in spin space. Applying a "magnetic field" along the $\hat{x}$ direction to this pseudospin should then induce Larmor precession, leading to periodic oscillations of the $z$-magnetization, corresponding to oscillations in the orbital population-imbalance $\mathcal{N}(p_x) - \mathcal{N}(p_y)$. Let us imagine we prepare the system in a certain initial state, and then suddenly quench to a state where we set $U_p = U_s = 0$, turn off all hoppings so $t = 0$, and turn on a "magnetic field" term

$$H_{\mathrm{mag}} = \sum_{\mathbf{r}} (-1)^{r_x+r_y}\lambda(\mathbf{r})\left[b_x^\dagger(\mathbf{r})b_y(\mathbf{r}) + b_y^\dagger(\mathbf{r})b_x(\mathbf{r})\right] \quad (9)$$

at time $\tau = 0$; we later discuss how to realize such a term in optical lattice experiments. The staggered sign $(-1)^{r_x+r_y}$ leads to a staggered coupling between the $p_x$- and $p_y$-orbitals. If initially a staggered superposition $p_x \pm e^{i\theta}p_y$ is prepared, this results in a rectification of all local Lamor precessions such that they add up to produce a macroscopic oscillation of the populations of the $p_x$- and $p_y$-orbitals. The $p$-orbital imbalance, $\Delta\mathcal{N}(\mathbf{r}) = b_x^\dagger(\mathbf{r})b_x(\mathbf{r}) - b_y^\dagger(\mathbf{r})b_y(\mathbf{r})$, evolves, within a Heisenberg picture, as

$$\frac{d\Delta\mathcal{N}(\mathbf{r},\tau)}{d\tau} = -i[\Delta\mathcal{N}(\mathbf{r},\tau), H_{\mathrm{mag}}] = -2\lambda(\mathbf{r})\mathcal{L}_z^{\mathrm{stag}}(\mathbf{r},\tau) \quad (10)$$

where $\mathcal{L}_z^{\mathrm{stag}} = \mathcal{L}_z(-1)^{r_x+r_y}$ is the staggered angular momentum operator whose evolution is in turn given by

$$\frac{d\mathcal{L}_z^{\mathrm{stag}}(\mathbf{r},\tau)}{d\tau} = 2\lambda(\mathbf{r})\Delta\mathcal{N}(\mathbf{r},\tau). \quad (11)$$

This leads to periodic oscillations of $\Delta N(\mathbf{r},\tau) = \langle\Delta\mathcal{N}(\mathbf{r},\tau)\rangle$ as

$$\Delta N(\mathbf{r},\tau) = \Delta N(\mathbf{r},0)\cos(2\lambda(\mathbf{r})\tau) - L_z^{\mathrm{stag}}(\mathbf{r},0)\sin(2\lambda(\mathbf{r})\tau)$$
$$\equiv A(\mathbf{r})\cos(2\lambda(\mathbf{r})\tau + \phi(\mathbf{r})). \quad (12)$$

where $\Delta N(\mathbf{r},0)$ and $L_z^{\mathrm{stag}}(\mathbf{r},0)$ denote the initial orbital magnetization and staggered angular momentum, respectively. Neglecting possible spatial inhomogeneity in $\lambda(\mathbf{r})$ and $\phi(\mathbf{r})$, by focusing at the trap center, we can set $\lambda(\mathbf{r}) = \lambda$ and $\phi(\mathbf{r}) = \phi$, and extract the initial angular momentum order from the amplitude $A(\mathbf{r})$ and the phase shift $\phi$ in the dynamics of the averaged number difference $\overline{\Delta N}(\tau) = \frac{1}{N_s}\sum_{\mathbf{r}}\Delta N(\mathbf{r},\tau)$ with $N_s$ being the number of lattice sites at the trap center, and $\overline{(\ldots)}$ denoting the spatial average of $(\ldots)$. The coefficient $\lambda$ can be directly read-off from the oscillation period $\tau_Q \equiv \pi/\lambda$. We emphasize here that $\overline{\Delta N}$ suitably averaged over the entire trap can be measured in time-of-flight experiments [1].

For a state with nonzero staggered angular momentum order, but no initial orbital population imbalance, i.e., $\Delta N(\mathbf{r},0) = 0$, such as our chiral fluids, we expect $\overline{\Delta N}(\tau)$ to oscillate with a nonzero amplitude, and a phase $\pm\pi/2$ whose sign will fluctuate from realization to realization, reflecting the spontaneous nature of time-reversal symmetry breaking. The amplitude of the signal will then be a direct measure of the staggered angular momentum order parameter, vanishing in a singular manner at the Ising phase transition which restores time-reversal symmetry. By contrast, a completely thermally disordered conventional normal fluid would have $\overline{\Delta N}(\tau) = 0$. A state with an initial orbital population imbalance but no angular momentum order, obtained by explicitly breaking the square lattice $C_4$ symmetry in the initial Hamiltonian as achieved in recent experiments, would exhibit oscillations with a nonsingular amplitude and a phase $\phi = 0$. Finally, if spontaneous time-reversal symmetry breaking exists in a system without $C_4$ symmetry, the amplitude of $\overline{\Delta N}(\tau)$ will be nonsingular while its phase will change in a singular manner, going from $\phi = \pm\pi/2$ in a completely ordered state to $\phi = 0$ at the time-reversal symmetry restoring phase transition. Since this quench induced orbital magnetization dynamics is inherently a non-interferometric probe of the angular momentum order, it suggests a simple and powerful method for measuring time-reversal symmetry breaking in superfluid *as well*

*as* non-superfluid chiral states. Our proposal thus significantly extends the earlier proposed quench dynamics approach for probing generic current orders [44, 45]. In the presence of superfluid order, our real space quench is analogous to the recent proposal of Cai *et al.,* [46] which proposes to extract the relative phase between the $p_x$ and $p_y$ orbitals by studying momentum spectra after applying a Raman pulse to the Bose condensate. However, our proposal differs in showing that the angular momentum order can be probed irrespective of long range phase coherence or sharp momentum peaks.

**Numerical Simulations of Quench Dynamics.** Our above analysis assumed that the quantum quench was complete, i.e., all tunnelings ($t$) and interactions ($U$) were entirely switched off when $H_{\mathrm{mag}}$ was switched on. We now show, using numerical simulations, that the coherent orbital oscillations are robust even with small nonzero tunnelings and interactions present after the quench, i.e., for an *incomplete* quench.

Since the scheme we are proposing here directly measures the local angular momentum order, it does not rely on the system dimensionality (beyond the assumption of long-range order). We therefore numerically simulate the zero temperature quench dynamics of a 1D model of $p$-orbital bosons, using both time-dependent Gutzwiller mean field theory [47] and time-dependent matrix product states (tMPS), finding good agreement at both weak and strong couplings and qualitatively similar conclusions at intermediate interaction strength. We then use the Gutzwiller mean field theory to also simulate the dynamics for the 2D case relevant to current experiments.

The Hamiltonian of the 1D system is [26]

$$H_{1D} = \sum_j \left[ t_\parallel b_x^\dagger(j) b_x(j+1) - t_\perp b_y^\dagger(j) b_y(j+1) + h.c. \right]$$
$$+ \sum_j \frac{U}{2} \left\{ n(j) \left[ n(j) - \frac{2}{3} \right] - \frac{1}{3} \mathcal{L}_z^2(j) \right\}, \quad (13)$$

where $j$ index lattice sites. The ground state phase diagram of this 1D system includes two types of Mott states at strong coupling: a chiral Mott with staggered angular momentum order, and a non-chiral Mott insulator. For weak correlations, it supports two types of SF ground states: a chiral superfluid with staggered angular momentum order and a non-chiral superfluid [26]. The chiral states have an order parameter $L_z^{\mathrm{stag}}(j) = \langle \mathcal{L}_z^{\mathrm{stag}}(j) \rangle$, with $\mathcal{L}_z^{\mathrm{stag}}(j) = (-1)^j \mathcal{L}_z(j)$, which is analogous to the 2D case. We start with different ground states of $H_{1D}$ and study their time evolution under a quantum quench which suddenly changes the Hamiltonian to $H_{1D} + \Delta H_{1D}$, where

$$\Delta H_{1D} = \lambda \sum_j (-1)^j \left[ b_x^\dagger(j) b_y(j) + b_y^\dagger(j) b_x(j) \right]. \quad (14)$$

The oscillatory dynamics of $\overline{L_z^{\mathrm{stag}}}$ and $\overline{\Delta N}$ is confirmed even for these entangled many-body states (Fig. 4). Since

the 1D geometry does not possess $C_4$ symmetry, we expect the different states to be distinguished by the phase shift $\phi$, not the amplitude, of the oscillatory dynamics. The chiral Mott and superfluid states develop a periodic motion with non-zero phase shift. The dynamics of non-chiral states indicate zero phase shift. In this way the chiral states can be distinguished from non-chiral states by measuring the phase shift, which is directly related to the angular momentum order parameter. Deep in the chiral superfluid state, the phase shift is $\phi = \pm\pi/2$, and it decreases in magnitude upon approaching the chiral-nonchiral critical point. The phase shift vanishes in a singular fashion at this quantum critical point, signaling that this phase transition associated with time-reversal symmetry can be probed by measuring the order parameter via the phase shift $\phi$.
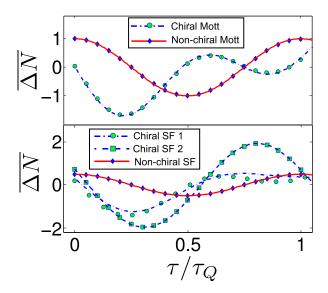


FIG. 4: Quench dynamics of one dimensional phases. Dots and lines are results of tMPS and Gutzwiller methods, respectively. The upper (bottom) panel shows dynamics of Mott (superfluid) states. The fillings for chiral and non-chiral Mott states, chiral SF 1, non-chiral SF and chiral SF 2 are $\langle n(\mathbf{r}) \rangle = 2, 1, 1.5, 0.5$ and $2$, respectively. For the chiral SF 2 state, we use $t_\parallel = 2t_\perp = U/3 = \lambda/10$; while for other states we use $t_\parallel = 9t_\perp = 0.045U = 0.09\lambda$. The time unit $\tau_Q$ is $\pi/\lambda$.

Comparing time-dependent Gutzwiller [48] and tMPS methods (Fig. 4), we find that the Gutzwiller approach captures orbital dynamics fairly well. We thus apply this approach to study orbital dynamics of the two dimensional system, as in experiments [1]. We have verified that a partial quench leads to long-lived $\Delta N$ oscillations as long as $t$ and $U$ are weak compared with the quench strength, i.e., $t/\lambda \ll 1$ and $U/\lambda \ll 1$. These results are shown in Fig. 5.

## Discussion

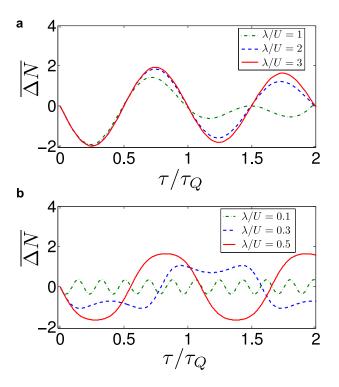In most cold atom experiments, the trap potential can induce a slowly varying inhomogeneity in the "magnetic

FIG. 5: Quench dynamics of two dimensional phases with various quench strengths via Gutzwiller approach. (a) and (b) show the evolution of $\Delta N$ for chiral Mott states (with $t_\parallel = t_\perp = 0.0125U_p$) and superfluid states ($t_\parallel = t_\perp = U_p$), respectively. The filling is $\langle n(\mathbf{r})\rangle = 2$. The time unit $\tau_Q$ is $\pi/\lambda$. Non-chiral phases (not shown) have $\Delta N = 0$, and do not exhibit any post-quench oscillations.

field" $\lambda$ as $\delta\lambda = \max\{\lambda(\mathbf{r})\} - \min\{\lambda(\mathbf{r})\}$. We expect the oscillations of the trap averaged number difference $\overline{\Delta N}$ to decay over a time-scale $\sim \frac{1}{\delta\lambda}$. Finally we emphasize that besides the angular momentum order parameter, the quantum quench proposal and a subsequent study of $\Delta N(\mathbf{r}, \tau)$ using in-situ microscopy can also yield correlation functions of $\mathcal{L}_z^{\mathrm{stag}}(\mathbf{r})$, from which the diverging correlation length near the transition from chiral Bose liquid to normal can be extracted.

## Methods

**Experimental Proposal for Quench.** To engineer the Hamiltonian $H_{\mathrm{mag}}$ of Eq. (9), we implement a quench potential $V_{\mathrm{mag}}(\mathbf{x})$ modulated in the $(1,1)$ direction in addition to the lattice potential giving rise to the quench Hamiltonian

$$H_{\mathrm{mag}} = \tag{15}$$
$$\sum_{\mathbf{r}}\left[\epsilon(\mathbf{r})\left(b_x^\dagger(\mathbf{r})b_y(\mathbf{r}) + h.c.\right) + \mu(\mathbf{r})\,n_p(\mathbf{r})\right],$$

with

$$\epsilon(\mathbf{r}) \approx \frac{\hbar}{4m\omega_0}\frac{\partial^2 V_{\mathrm{mag}}\left(\mathbf{r} + l\left[\frac{\hat{a}_x + \hat{a}_y}{\sqrt{2}}\right]\right)}{a^2 \partial l^2}\Big|_{l\to 0}, \tag{16}$$

which is valid in the tight binding regime when the quench potential is weak as compared to the original optical lattice (see Supplementary Information). Here, $\omega_0$ is the harmonic oscillator frequency of the lattice wells hosting the $p$-orbitals, and $a \equiv |\hat{a}_x| = |\hat{a}_y|$ is the lattice constant. Since the local density operator of the $p$-orbitals $n_p(\mathbf{r})$ commutes with $\Delta\mathcal{N}(\mathbf{r})$ and $\tilde{\mathcal{L}}_z(\mathbf{r})$, it does not contribute to the dynamics of $\Delta\mathcal{N}(\mathbf{r})$, and hence may be neglected. This is verified in our Gutzwiller simulations. We choose the quench potential as

$$V_{\mathrm{mag}}(\mathbf{x}) = -\Gamma\cos^2\left(\frac{2\nu+1}{4}(\hat{K}_x + \hat{K}_y)\cdot\mathbf{x}\right), \tag{17}$$

with some integer $\nu \geq 0$, a positive amplitude $\Gamma$, and $\hat{K}_x$, $\hat{K}_y$ denoting the primitive vectors of the reciprocal lattice ($\hat{a}_i\cdot\hat{K}_j = 2\pi\,\delta_{ij}$ with $i,j \in \{x,y\}$). The quench potential provides a lattice along the $(1,1)$ direction, and it breaks both $C_4$ symmetry and mirror symmetries in the $x$ and $y$ directions. The potential is minimal at every second site of the Bravais lattice at positions $\mathbf{r}(=r_x\hat{a}_x + r_y\hat{a}_y)$ with even $r_x + r_y$ and it is maximal for all adjacent sites specified by odd $r_x + r_y$. Hence, the second derivative in Eq. (16) produces the alternating sign $(-1)^{r_x+r_y}$ required for realization of the quench Hamiltonian in Eq. (9). Combining Eqs. (17) and Eq. (16) yields

$$\epsilon(\mathbf{r}) = \frac{E_{\mathrm{rec}}}{\hbar\omega_0}\frac{\Gamma}{4}(2\nu+1)^2(-1)^{r_x+r_y}, \tag{18}$$

with $E_{\mathrm{rec}} \equiv \hbar^2 k^2/2m$ denoting the single photon recoil energy for photons with wave number $k = \frac{1}{2}|\hat{K}_x + \hat{K}_y|$.

The lattice potential together with the corresponding quench potential can be realized by superlattice techniques demonstrated in several experiments [1, 24, 36, 49]. For example, following Ref. [1], the lattice potential arises via two optical standing waves oriented along the $(1,1)$ and $(1,-1)$ axes with a wave number $k = \frac{1}{2}|\hat{K}_x + \hat{K}_y| = 2\pi/1064$ nm. The corresponding quench lattice requires an additional standing wave along the $(1,1)$ axis with wave number $k' = \frac{2\nu+1}{2}k$. Hence, the case $\nu = 1$ requires $k' = \frac{3}{2}k \approx 2\pi/709$ nm, which is experimentally readily provided by diode laser sources. Both standing waves along the $(1,1)$-direction may be derived by retro-reflecting two parallelly propagating laser beams with wave numbers $k$ and $k'$ by the same mirror. In order to prepare the required spatial relative phase of the two lattices, $k'$ may be slightly detuned from the precise ratio $k'/k = \frac{3}{2}$.

**Monte Carlo simulations.** We carry out the Monte Carlo study of the Hamiltonian $H_{\mathrm{phase}}^{\mathrm{eff}}$ in Eq. (8) using a Metropolis sampling of the phase configurations $\{\theta_x(\mathbf{r}), \theta_y(\mathbf{r})\}$, with $10^7$ sweeps to equilibrate the system at each temperature, and averaging all observables over $10^8$ configurations. To study the phase diagram of $H_{\mathrm{phase}}^{\mathrm{eff}}$, we focus on the angular momentum order parameter, the superfluid stiffness, and the momentum distribution, all of which are discussed below.

The angular momentum order parameter in the phase-only effective model takes the form of $\mathcal{M} = \sum_{\mathbf{r}}(-1)^{r_x+r_y}\sin(\theta_x(\mathbf{r}) - \theta_y(\mathbf{r}))$ and compute its Binder cumulant [42] $\mathcal{B}_L(\mathcal{L}_z) = 1 - \frac{\langle\mathcal{M}^4\rangle}{3\langle\mathcal{M}^2\rangle^2}$. The universal order parameter distribution at renormalization group fixed points leads to universal values of $\mathcal{B}_{L\to\infty}$; on finite size systems, this yields Binder cumulant curves which cross at the critical point associated with angular momentum ordering. The critical value $B^*$ of the Binder cumulant is well-known to be universal, independent of lattice structure and details of the Hamiltonian, and depending only on the aspect ratio and boundary conditions used in the simulations. For periodic boundary conditions on $L \times L$ lattices, $B^* \approx 0.61069$ for the 2D Ising universality class.

The superfluid stiffness $\rho_s$ is defined as the change in the free energy density in response to a boundary condition twist; for $H_{\text{phase}}^{\text{eff}}$, it is explicitly given by

$$\rho_s(T) = \frac{1}{N}(\langle\mathcal{K}_x\rangle - \frac{1}{T}\langle\mathcal{I}_x^2\rangle) \tag{19}$$

$$\mathcal{K}_x = -2J_\parallel\sum_{\mathbf{r}}\cos(\Delta_x\theta_x(\mathbf{r})) + 2J_\perp\sum_{\mathbf{r}}\cos(\Delta_x\theta_y(\mathbf{r})) \tag{20}$$

$$\mathcal{I}_x = 2J_\parallel\sum_{\mathbf{r}}\sin(\Delta_x\theta_x(\mathbf{r})) - 2J_\perp\sum_{\mathbf{r}}\sin(\Delta_x\theta_y(\mathbf{r})) \tag{21}$$

where $\langle\cdots\rangle$ refers to the thermal average. At a BKT transition, $\rho_s(T)$ jumps to zero, with $\rho_s(T_{\text{BKT}})/T_{\text{BKT}} = 2/\pi$, a universal value. On finite size systems, the universal superfluid stiffness jump gets severely rounded, and a careful finite size scaling is required to extract $T_{\text{BKT}}$. Based on the KT renormalization group equations, Weber and Minnhagen have shown [43] that $\rho_s(T_{\text{BKT}}, L)$ scales as

$$\rho_s(T_{\text{BKT}}, L) = \rho_s(T_{\text{BKT}}, \infty)(1 + \frac{1}{2\log L + c}) \tag{22}$$

where $c$ is a non-universal number. It is well-known that fitting to this log-scaling form at different temperatures leads to an error which exhibits a steep minimum at $T_{\text{BKT}}$, enabling us to extract $T_{\text{BKT}}$ from our simulations. An unbiased fit to $\rho_s(T)/T$, using a two-parameter scaling form,

$$\frac{\rho_s(T_{\text{BKT}}, L)}{T_{\text{BKT}}} = a(1 + \frac{1}{2\log L + c}) \tag{23}$$

also enables one to confirm the universal jump at the $T_{\text{BKT}}$ identified by the error minimum. Using this, we find $a \approx 0.64$ from our simulations, in very good agreement with the KT value $2/\pi = 0.6366....$

**Author contributions**

X.L. and A.P. conceived and evolved the theoretical ideas in discussion with W.V.L. A.H. examined and improved the experimental protocol. X.L. and A.P. performed numerical simulations. All authors worked on theoretical analysis and contributed in completing the paper.

**Author Information**

The authors declare no competing financial interests. Correspondence and requests for material should be sent to w.vincent.liu@gmail.com. Supplementary information accompanies this paper.

# Supplementary Information

## Formation and detection of a chiral orbital Bose liquid in an optical lattice

### DERIVATION OF THE QUENCH STRENGTH

The induced coupling between $p_x$ and $p_y$ orbitals by the quench potential $V_{\mathrm{mag}}(\mathbf{r})$ is

$$H_{\mathrm{mag}} = \sum_{\alpha\beta,\mathbf{r}} g_{\alpha\beta}(\mathbf{r}) b_\alpha^\dagger(\mathbf{r}) b_\beta(\mathbf{r}), \tag{S1}$$

with

$$g_{\alpha\beta}(\mathbf{r}) = \int d^2\mathbf{x}\, w_\alpha^*(\mathbf{x}-\mathbf{r}) V_{\mathrm{mag}}(\mathbf{x}) w_\beta(\mathbf{x}-\mathbf{r}),$$

where $w_{\alpha=x/y}(\mathbf{x})$ are Wannier functions for $p_x$ and $p_y$ bands. The Wannier functions may be approximated by localized harmonic oscillator wavefunctions, with their widths determined by the harmonic oscillator frequency $\omega_0$. This approximation is valid in the tight binding regime to estimate local quantities, as $g_{\alpha\beta}$. For simplicity, calculations are done in a transformed basis defined by

$$\begin{bmatrix} \tilde{b}_x \\ \tilde{b}_y \end{bmatrix} = \begin{bmatrix} b_x + b_y \\ b_x - b_y \end{bmatrix} / \sqrt{2}. \tag{S2}$$

In this basis, the induced coupling reads $\tilde{g}_{\alpha\beta} \tilde{b}_\alpha^\dagger \tilde{b}_\beta$, with

$$\tilde{g}_{\alpha\beta}(\mathbf{r}) = \int d\tilde{x}\, d\tilde{y}\, w_\alpha^*(\tilde{x},\tilde{y}) \tilde{V}_{\mathrm{mag}}(\tilde{x}) w_\beta(\tilde{x},\tilde{y}), \tag{S3}$$

where $\tilde{x} = [(x+y)-(r_x+r_y)a]/\sqrt{2}$, $\tilde{y} = [x-y-(r_x-r_y)a]/\sqrt{2}$ , with $a$ the lattice constant. And the potential $V_{\mathrm{mag}}(\mathbf{x})$ in the transformed coordinates reads as $\tilde{V}_{\mathrm{mag}}(\tilde{x}) = -\Gamma \cos^2[\frac{(2m+1)k}{2}\tilde{x}]$, with $k = \frac{1}{2}|\hat{K}_x + \hat{K}_y|$ and $a = \frac{\sqrt{2}\pi}{k}$ denoting the lattice constant. Since Wannier functions are localized, we can approximate the quench potential by

$$\tilde{V}_{\mathrm{mag}}(\tilde{x}) = V_{\mathrm{mag}}(\mathbf{r}) + \frac{1}{2}\tilde{x}^2 \frac{d^2\tilde{V}_{\mathrm{mag}}}{d\tilde{x}^2}\Big|_{\tilde{x}=0}. \tag{S4}$$

The derivative term may be rewritten as

$$\frac{d^2\tilde{V}_{\mathrm{mag}}}{d\tilde{x}^2}\Big|_{\tilde{x}=0} = \frac{1}{a^2} \frac{\partial^2 V_{\mathrm{mag}}\left(\mathbf{r} + l\frac{\hat{a}_x+\hat{a}_y}{\sqrt{2}}\right)}{\partial l^2}\Big|_{l=0}. \tag{S5}$$

From Eq. (S3) and Eq. (S4), we get

$$[\tilde{g}] = g^{(d)}(\mathbf{r})\mathbb{I} + \epsilon(\mathbf{r})\sigma_z, \tag{S6}$$

with

$$\epsilon(\mathbf{r}) = \frac{\hbar}{4m\omega_0} \frac{\partial^2 V_{\mathrm{mag}}\left(\mathbf{r} + l\frac{\hat{a}_x+\hat{a}_y}{\sqrt{2}}\right)}{a^2 \partial l^2}\Big|_{l=0}, \tag{S7}$$

and $\mathbb{I} = \begin{bmatrix} 1 & 0 \\ 0 & 1 \end{bmatrix}$, $\sigma_z = \begin{bmatrix} 1 & 0 \\ 0 & -1 \end{bmatrix}$.

Transforming back to the original basis, we get a coupling term

$$\sum_{\mathbf{r}} \epsilon(\mathbf{r}) \left[ b_x^\dagger(\mathbf{r}) b_y(\mathbf{r}) + h.c. \right]. \tag{S8}$$

In Gutzwiller simulations, the neglected diagonal part is studied and we find that its modification of the orbital dynamics is minor.

[1] G. Wirth, M. Ölschläger, and A. Hemmerich, Nature Physics **7**, 147 (2011).

[2] M. Ölschläger, T. Kock, G. Wirth, A. Ewerbeck, C. M.

Smith, and A. Hemmerich, New Journal of Physics **15**, 083041 (2013).

[3] X. Li, E. Zhao, and W. V. Liu, Phys. Rev. A **83**, 063626 (2011).

[4] L. Onsager, Phys. Rev. **65**, 117 (1944).

[5] J. Bednorz and K. Müller, Zeitschrift für Physik B Condensed Matter **64**, 189 (1986).

[6] Y. Kamihara, H. Hiramatsu, M. Hirano, R. Kawamura, H. Yanagi, T. Kamiya, and H. Hosono, Journal of the American Chemical Society **128**, 10012 (2006), pMID: 16881620.

[7] R. von Helmolt, J. Wecker, B. Holzapfel, L. Schultz, and K. Samwer, Phys. Rev. Lett. **71**, 2331 (1993).

[8] G. M. Luke, Y. Fudamoto, K. M. Kojima, M. I. Larkin, J. Merrin, B. Nachumi, Y. J. Uemura, Y. Maeno, Z. Q. Mao, Y. Mori, et al., Nature (London) **394**, 558 (1998).

[9] Y. Tokura and N. Nagaosa, Science **288**, 462 (2000).

[10] M. A. Lewenstein and W. V. Liu, Nature Physics **7**, 101 (2011).

[11] E. Zhao and W. V. Liu, Phys. Rev. Lett. **100**, 160403 (2008).

[12] Z. Zhang, H.-H. Hung, C. M. Ho, E. Zhao, and W. V. Liu, Phys. Rev. A **82**, 033610 (2010).

[13] Z. Cai, Y. Wang, and C. Wu, Phys. Rev. A **83**, 063621 (2011).

[14] H.-H. Hung, W.-C. Lee, and C. Wu, Phys. Rev. B **83**, 144506 (2011).

[15] Z. Zhang, X. Li, and W. V. Liu, Phys. Rev. A **85**, 053606 (2012).

[16] K. Sun, W. V. Liu, A. Hemmerich, and S. Das Sarma, Nature Physics **8**, 67 (2012).

[17] X. Li, E. Zhao, and W. V. Liu, Nature Commun **4**, 1523 (2013).

[18] A. Isacsson and S. M. Girvin, Phys. Rev. A **72**, 053604 (2005).

[19] W. V. Liu and C. Wu, Phys. Rev. A **74**, 013607 (2006).

[20] A. B. Kuklov, Phys. Rev. Lett. **97**, 110405 (2006).

[21] L.-K. Lim, C. M. Smith, and A. Hemmerich, Phys. Rev. Lett. **100**, 130402 (2008).

[22] V. M. Stojanović, C. Wu, W. V. Liu, and S. Das Sarma, Phys. Rev. Lett. **101**, 125301 (2008).

[23] Q. Zhou, J. V. Porto, and S. Das Sarma, Phys. Rev. B **83**, 195106 (2011).

[24] P. Soltan-Panahi, D.-S. Lühmann, J. Struck, P. Windpassinger, and K. Sengstock, Nature Physics **8**, 71 (2012).

[25] Z. Cai and C. Wu, Phys. Rev. A **84**, 033635 (2011).

[26] X. Li, Z. Zhang, and W. V. Liu, Phys. Rev. Lett. **108**, 175302 (2012).

[27] F. Hébert, Z. Cai, V. G. Rousseau, C. Wu, R. T. Scalettar, and G. G. Batrouni, Phys. Rev. B **87**, 224505 (2013).

[28] P. Hauke, E. Zhao, K. Goyal, I. H. Deutsch, W. V. Liu, and M. Lewenstein, Phys. Rev. A **84**, 051603 (2011).

[29] C. Wu, Mod. Phys. Lett. B **23**, 1 (2009).

[30] A. P. Mackenzie and Y. Maeno, Rev. Mod. Phys. **75**, 657 (2003).

[31] C. Kallin, Reports on Progress in Physics **75**, 042501 (2012).

[32] R. Nandkishore, Phys. Rev. B **86**, 045101 (2012).

[33] C. M. Varma, Phys. Rev. B **61**, R3804 (2000).

[34] S. Chakravarty, R. B. Laughlin, D. K. Morr, and C. Nayak, Phys. Rev. B **63**, 094503 (2001).

[35] B. Fauqué, Y. Sidis, V. Hinkov, S. Pailhès, C. T. Lin, X. Chaud, and P. Bourges, Phys. Rev. Lett. **96**, 197001 (2006).

[36] S. Folling, S. Trotzky, P. Cheinet, M. Feld, R. Saers, A. Widera, T. Muller, and I. Bloch, Nature **448**, 1029 (2007).

[37] L. Tarruell, D. Greif, T. Uehlinger, G. Jotzu, and T. Esslinger, Nature **483**, 302 (2012).

[38] M. Ölschläger, G. Wirth, T. Kock, and A. Hemmerich, Phys. Rev. Lett. **108**, 075302 (2012).

[39] A. Dhar, M. Maji, T. Mishra, R. V. Pai, S. Mukerjee, and A. Paramekanti, Phys. Rev. A **85**, 041602 (2012).

[40] A. Dhar, T. Mishra, M. Maji, R. V. Pai, S. Mukerjee, and A. Paramekanti, Phys. Rev. B **87**, 174501 (2013).

[41] M. P. Zaletel, S. A. Parameswaran, A. Rüegg, and E. Altman, ArXiv e-prints (2013), 1308.3237.

[42] K. Binder, Zeitschrift für Physik B Condensed Matter **43**, 119 (1981).

[43] H. Weber and P. Minnhagen, Phys. Rev. B **37**, 5986 (1988).

[44] M. Killi and A. Paramekanti, Phys. Rev. A **85**, 061606 (2012).

[45] M. Killi, S. Trotzky, and A. Paramekanti, Phys. Rev. A **86**, 063632 (2012).

[46] Z. Cai, L.-M. Duan, and C. Wu, Phys. Rev. A **86**, 051601 (2012).

[47] G. Seibold and J. Lorenzana, Phys. Rev. Lett. **86**, 2605 (2001).

[48] M. Snoek and W. Hofstetter, Phys. Rev. A **76**, 051603 (2007).

[49] M. Anderlini, P. J. Lee, B. L. Brown, J. Sebby-Strabley, W. D. Phillips, and J. V. Porto, Nature **448**, 452 (2007).